Available online at www.sciencedirect.com

ScienceDirect

Ceramics International 40 (2014) 289–296

CERAMICS INTERNATIONAL

www.elsevier.com/locate/ceramint

Ionothermal synthesis and characterization of Li_2MnSiO_4/C composites as cathode materials for lithium-ion batteries

Xueliang Li[a,b,*], Yunfu Liu[a,b], Zhenghui Xiao[a,b], Wei Guo[a,b], Rui Zhang[a,b]

[a]School of Chemical Engineering, Hefei University of Technology, Hefei 230009, PR China
[b]Anhui Key Laboratory of controllable Chemical Reaction and Material, Chemical Engineering, Hefei 230009, PR China

Received 20 April 2013; received in revised form 31 May 2013; accepted 31 May 2013
Available online 7 June 2013

Abstract

Li_2MnSiO_4 powders have been synthesized under mild conditions via an ionothermal synthesis method in ionic liquids of 1-ethyl-3-methylimidazolium tetrafluoroborate ([EMIM]BF_4) and 1-butyl-3-methylimidazolium tetrafluoroborate ([BMIM]BF_4), respectively, and then Li_2MnSiO_4/C cathode materials were prepared by solid-state reaction using sucrose as carbon source at high temperature. The structures and morphologies were characterized by X-ray diffraction (XRD), scanning electron microscopy (SEM), and transmission electron microscopy (TEM). Li_2MnSiO_4 powders prepared in two ionic liquids present different morphologies and particle sizes and the length of alkyl chains on the imidazole ring plays important role in forming the size and morphology of material. The Li_2MnSiO_4 can crystallize in an orthorhombic structure with a space group of $Pmn2_1$ and form uniform material with the size of primary particle ranging from 50 to 80 nm, and Li_2MnSiO_4/C composites prepared via precursors produced in [BMIM]BF_4 achieved the excellent electrochemical performance with an initial discharge capacity of 218.2 mAh g^{-1}, and retained an effective discharge of 175.7 mAh g^{-1} after 50 cycles. Results reveal that the ionothermal synthesis could be a promising new route in preparing Li_2MnSiO_4 cathode material for lithium-ion batteries in decreasing particle size, reducing reaction conditions, and improving electrochemical performance.

Keywords: Lithium-ion batteries; Li_2MnSiO_4; Ionothermal synthesis; Ionic liquid

1. Introduction

The urgent need for large-scale batteries motivates the continuous research and innovations of new materials for lithium-ion batteries. Many materials such as $LiCoO_2$, $LiMn_2O_4$, $LiNiO_2$ and $LiFePO_4$ have been widely studied [1–4]. Li_2MSiO_4 (M=Mn, Fe, Co, and Ni) [5–8] could fulfill various safety, price, environmental benefits. Comparing with $LiFePO_4$, Li_2MnSiO_4 efficiently offers sufficient specific capacity and energy density [9–15]. It was certified that Li_2MnSiO_4 has two lithium ions per formula unit, suggesting a higher theoretical capacity (333 mAh g^{-1}) than phosphates.

So far, much effort has been made by many researchers to circumvent low electronic conductivity and structural instability of the lithium orthosilicate. Several methods were employed such as carbon coating [16–18], particle size reduction [19,20] and super-valent or isovalent metal doping [21,22]. Although progress has been made by these methods, the overall performance of Li_2MnSiO_4 is still not sufficient for practical battery applications. On one hand, carbon coating is a simple, effective and cost-saving method to increase electronic conductivity which has been reported by Deng [5]. On the other hand, improving the structural stability of Li_2MnSiO_4 becomes the key for application of this electrode material. In the literature, there are several synthetic approaches for preparing Li_2MnSiO_4, namely solid-state reaction [10,21], sol–gel synthesis [5,12,19] and hydrothermal synthesis [8,23]. For instance, Gummow et al. [10] synthesized Li_2MnSiO_4 via solid-state reaction route, and the material showed that 1.3 lithium ions per formula unit can be extracted in the first charge cycle. Particle size reduction has been carried out via the sol–gel method [5]. Luo et al. [8] synthesized lithium orthosilicate by hydrothermal method and found it stable and superior cycling performance.

For the solid-state process, heating solid reactant mixtures at high temperature and long reaction time would result in the

*Corresponding author at: School of Chemical Engineering, Hefei University of Technology, Hefei 230009, PR China. Tel.: +86 551 2901450; fax: +86 551 2901450.
E-mail address: xueliangli2005@163.com (X. Li).

0272-8842/$ - see front matter © 2013 Elsevier Ltd and Techna Group S.r.l. All rights reserved.
http://dx.doi.org/10.1016/j.ceramint.2013.05.138

aggregation and large particle size of the final product. The sol–gel method can effectively control the reaction conditions, the yield products become high purity and homogeneity. Also the hydrothermal reaction provides good control to the reaction procedure, but it requires the cumbersome use of autoclaves. Considering the advantages and disadvantages of the above-mentioned methods, we propose the ionothermal method [24–26], which provides a new method to synthesize materials in ionic liquid medium and presents many advantages such as recycling, safety, low-temperature and ambient pressure. The reactants could be completely dissolved in ionic liquids at room temperature. The formation of bonds between the anion and cation of the ionic liquids and the cross-coupling interactions between the cation and mesh framework have a strong template effect. In addition, ionic liquids could be used as structure-directing agents to induce the formation of the structure of the product, and also protect the structure of nanocrystalline Li_2MnSiO_4. We synthesized Li_2MnSiO_4 materials by choosing imidazolium-based ionic liquids as reaction mediums for their advantages with high thermal stability, chemical stability, and negligible volatility. In this work, we will mainly focus on selecting two different imidazolium-based ionic liquids of 1-ethyl-3-methylimidazolium tetrafluoroborate ([EMIM]BF_4) and 1-butyl-3-methylimidazolium tetrafluoroborate ([BMIM]BF_4) to prepare uniform nanostructured Li_2MnSiO_4/C. Then, we discussed the reaction mechanism of different imidazolium-based ionic liquids on the size, morphology and structural stability. Especially we studied electrochemical performances of these calcinated powders [25] for high calcination temperature could improve the products of stable crystal and reduce impurities [10,27]. Electrochemical results show that Li_2MnSiO_4/C cathodes exhibited a promising improvement in terms of reversible capacity and cycling performance.

2. Experimental

The preparation process of Li_2MnSiO_4/C sample was as follows: tetraethyl orthosilicate (TEOS), $Mn(CH_3COO)_2{\bullet}2H_2O$ and $LiCH_3COO{\bullet}2H_2O$, in a stoichiometric ratio1:1:2, were stirred at 190 °C for 24 h in two different ionic liquids. After the reaction, Li_2MnSiO_4 precursor was cooled to room temperature, separated by centrifugal, repeated washing by distilled water and absolute alcohol, and dried at 80 °C for 6 h. The precursor powders prepared in [EMIM]BF_4 and [BMIM]BF_4 are labeled as M1 and M2, respectively. The products were ball milled with a certain amount of sucrose (10%, wt) for 0.5 h and calcinated at 600 °C, 700 °C and 750 °C protected by highly pure argon for 4 h. The obtained products were named as Li_2MnSiO_4/C-1 and Li_2MnSiO_4/C-2 prepared in [EMIM]BF_4 and [BMIM]BF_4, respectively.

After each experiment, these ionic liquids were recovered and regenerateed according to the followed process so that they could be used again. The process first consists in twice washing the reaction supernatant with concentrated HCl solutions in order to get rid of traces of solid impurity that could remain after centrifugation. Afterward, the supernatant is repeatedly washed with water to eliminate HCl traces, and then diluted with dichloromethane (CH_2Cl_2) to separate it from water. Finally, these ionic liquid can be used again for a new synthesis after being washed and dried, which is a plus from an economical point of view.

The crystalline phase of prepared powders was identified by the X-ray powder diffraction (XRD, Rigaku D/max-IIB) using a Cu-K_α radiation and operating at 40 kV, and 100 mA in the scan range 2θ=10–70°. The surface morphology and structural properties of the materials were studied by scanning electron microscopy (SEM, JEOL-JSM5610) and transmission electron microscopy (TEM, JEOL-JEM2010F).

The cathode electrodes were fabricated from a mixture of Li_2MnSiO_4/C material, conductive agent acetylene black and polyvinylidene fluoride (PVDF) in a ratio of 8:1:1. Then the N-methyl-pyrrolidone (NMP) as binder solvent was used to make the slurry of the mixtures. After being homogenized on the thin aluminum current collector, and dried under vacuum at 80 °C for 10 h, the electrode was being punched out into disks containing 10–12 mg active materials. The electrochemical cells were prepared using button cells. Lithium sheets were used as counter electrodes, and Celgard2400 polypropylene (PP) films were used as separators. The cell assembly process was carried out in an argon-filled glove box. 1 mol L^{-1} $LiPF_6$ in a mixture of ethylene carbonate (EC) and dimethyl carbonate (DMC) (1:1 volume ratio) were used as the electrolyte solution. The cells were examined by using the Land CT2001A charge and discharge system (Wuhan Jinnuo Electronics Co., Ltd. China) at rates of 0.1, 1, and 5 C between 2.5 and 4.5 V at room temperature. The specific capacities were calculated based on the weight of Li_2MnSiO_4/C and the electrochemical impedance measurements were carried out with a CHI 660B electrochemical workstation.

3. Results and discussion

3.1. XRD phase analysis

Fig. 1 shows XRD patterns of the M1 and M2 powders that synthesized under the mild conditions of low-temperature and ambient pressure. It is found that these precursors present crystalline state, and are noticed a stronger diffraction peak at 2θ=16.5°, which can be indexed as Li_2MnSiO_4 phase on the basis of orthorhombic unit cell with space group $Pmn2_1$. However, the two strong peaks around 2θ=19° and 27° easily observed in the pattern of both powders, which can be related to certain distinguishable characteristics of Li_2SiO_3 phase, and around 2θ=41°, corresponding to MnO [27]. Hence, Fig. 1 shows various weak XRD peaks corresponding to a low-crystalline and multi-component character. These precursors need further calcinating to obtain well-crystallized Li_2MnSiO_4. Moreover, we can also see some differences in the peak position, intensity, and full width at half maximum (FWHM) among the XRD patterns of these precursors. It is obviously seen that the FWHM of M2 is larger than that of M1, indicating the size of M2 powders is smaller than that of M1 powders from Fig. 1.

Fig. 2 shows XRD patterns of the obtained Li_2MnSiO_4/C powders mixture treated in a tubular furnace at 600, 700, and 750 °C for 4 h in flowing argon. Sucrose was used as the carbon source in the high-heat synthetic process. The XRD patterns suggest that all Li_2MnSiO_4 samples are indexed on the basis of orthorhombic unit cell with space group $Pmn2_1$, which are in good agreement with the literature values [9,14]. It has been noticed that the preparation of pure phase Li_2MnSiO_4 is complicated from this study and the previous reports [19], a few small reflections in the XRD data are accounted for with the inclusion of MnO as a minor impurity phase. Also, no carbon phase can be detected in these Li_2MnSiO_4/C composites, indicating that carbon generated from sucrose is amorphous and its presence does not influence the crystal structure of Li_2MnSiO_4. The XRD of Li_2MnSiO_4 prepared at 600 °C shows all the characteristic peaks. The unobvious difference in XRD responses between the samples calcinated at 700 °C and 750 °C suggests that the heat treatment process does not affect the crystal structure of the materials. The crystal structure of samples calcinated at 750 °C is most stable, which indicates that higher crystallinity of the regenerated sample is favored by higher temperature. Therefore, a regeneration temperature of 750 °C is selected in this study. It should be noticed from Fig. 2(b) that a strong peak around $2\theta = 16.5°$ can be easily observed, which show more well-crystallized structure of Li_2MnSiO_4/C-2 material.

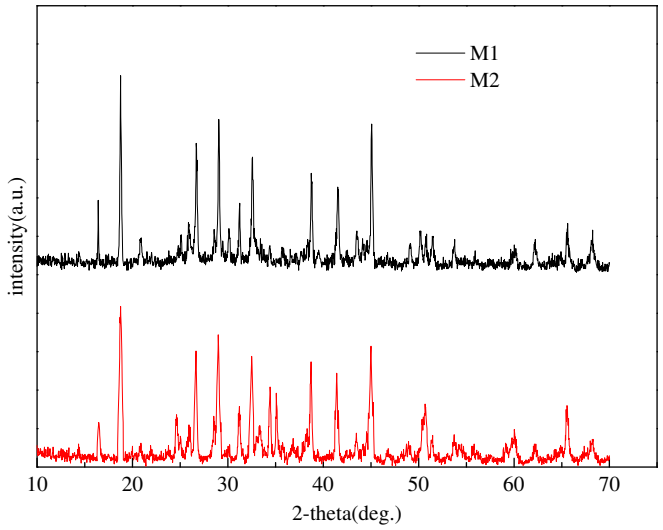

Fig. 1. XRD patterns of M1 and M2 powders.

3.2. SEM and TEM morphology analysis

Fig. 3 shows the particle shapes and morphologies of precursors and Li_2MnSiO_4/C. As shown in Fig. 3(a) and (e), both precursors (50–80 nm), composed of small primary particles, are irregularly-shaped and uniformly dispersed. Also, particle size and pore size of M2 are smaller than those of M1. These precursors show different morphologies and particle sizes, which may have significant influence on the characteristics of the final products after heat treatment. This can result in a clear difference in porosity. In Fig. 4, the specific surface area and pore size distribution of M1 and M2 were determined with Brunauer–Emmett–Teller (BET) and BJH. Due to the tensile strength effect (TSE) phenomenon according to the BJH model, an abnormal narrow distribution of real pores at 3.8 nm would show in two desorption branches [28]. The BET surface area of the M2 sample (25.1 $m^2\ g^{-1}$) is more than that of the M1 sample (16.6 $m^2\ g^{-1}$), which indicates that the M2 sample is more porous than the M1 sample. So porosity has a significant effect on the growth of well-crystallized Li_2MnSiO_4. For a highly porous material, these primary particles can easily gather together, and also the electrolyte can easily penetrate into the pores to enlarge the area for electrode reaction. Therefore, better electrochemical performance can be expected for the Li_2MnSiO_4-2 sample than the Li_2MnSiO_4-1 sample, which is confirmed by the electrochemical characterization [13]. Diameter of these nanocrystallines, in Fig. 3(b) and (f) (600 °C) ranging from 120 to 150 nm, are greater than those in Fig. 3(a) and (e). The remarkable point is that all of these particles pile up and grow in the same way during the calcining step. At the end, greater and well-crystallized

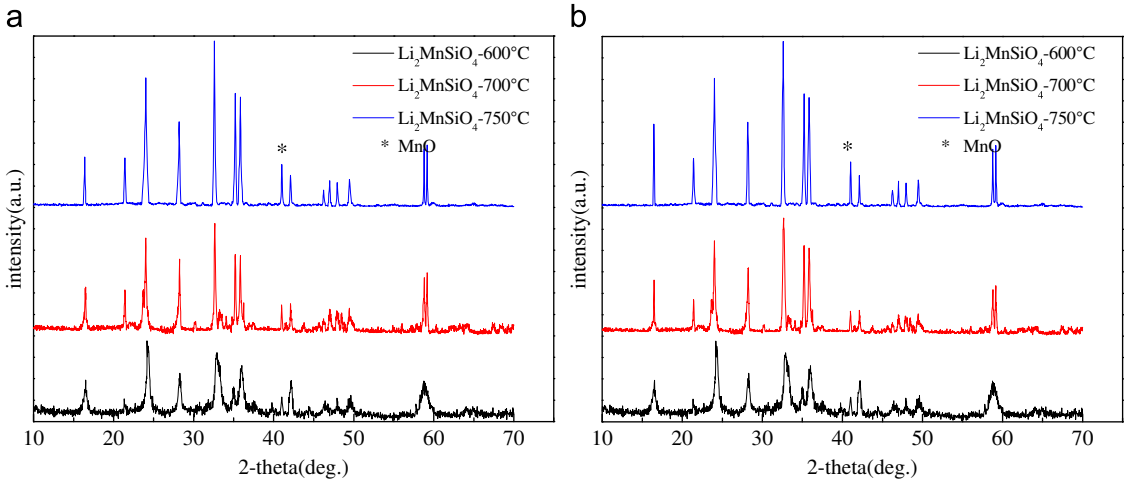

Fig. 2. XRD patterns of the prepared Li_2MnSiO_4/C-1 (a) and Li_2MnSiO_4/C-2 (b).

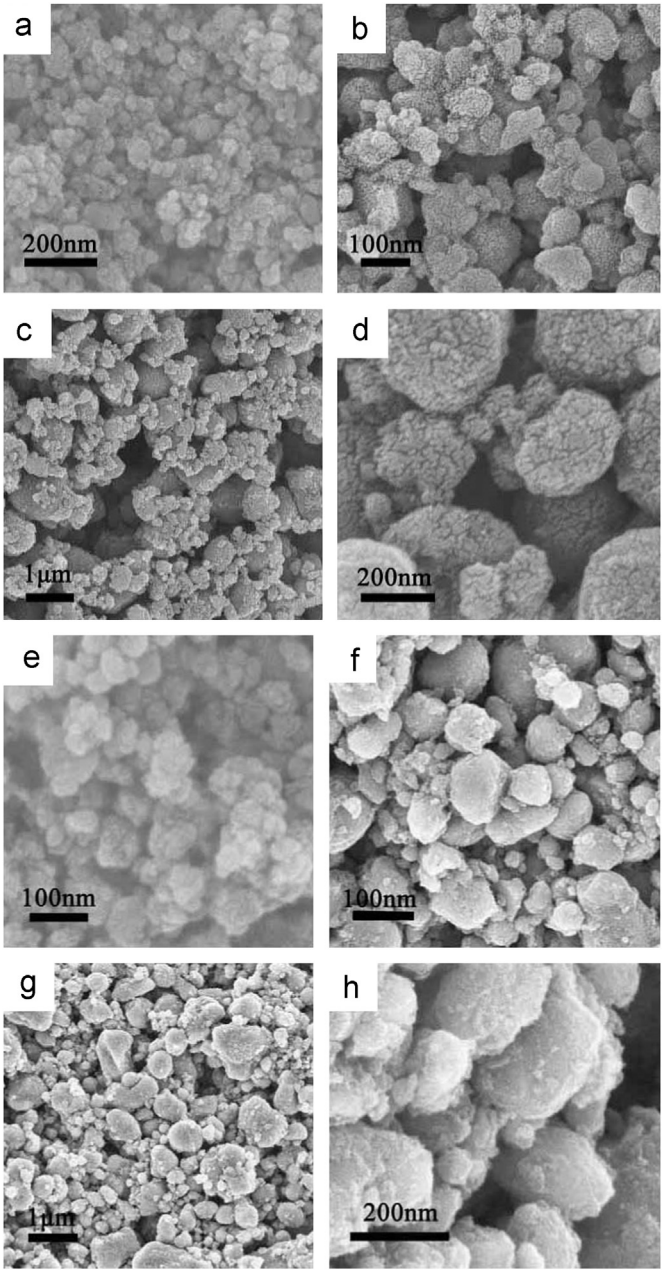

Fig. 3. SEM images of precursors (a and e), Li_2MnSiO_4/C-1 (b–d) and Li_2MnSiO_4/C-2(f–h): (a) M1 and (e) M2, (b) and (f) were fired at 600 °C, (c) and (g) were fired at 700 °C, (d) and (h) were fired at 750 °C.

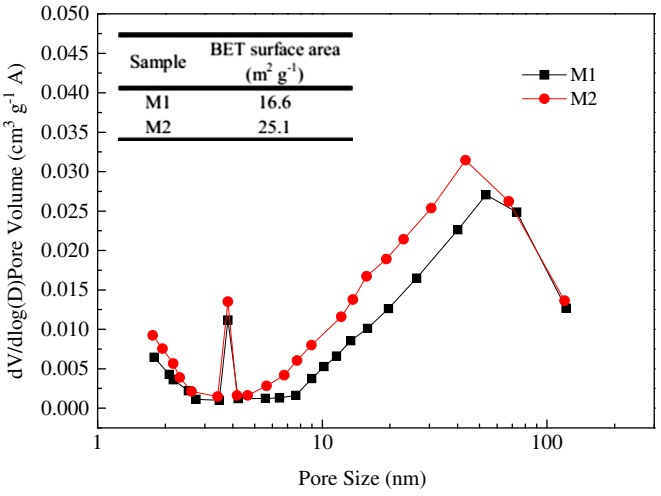

Fig. 4. Pore-size distribution and specific surface area of M1and M2.

Table 1
Different properties of two ionic liquids ([EMIM]BF_4 and [BMIM]BF_4).

Title	Viscosity (cP)	Interface tension (mJ m^{-2})
[EMIM]BF_4	153	50.4
[BMIM]BF_4	233	43.9

powders were prepared at 750 °C and their diameters range from 180 to 280 nm in Li_2MnSiO_4/C-1 sample (Fig. 3(d)) and 150 to 250 nm in Li_2MnSiO_4/C-2 sample (Fig. 3(h)). Based on these studies, we chose the samples prepared at 750 °C to do other tests. As a result of uniform size and large specific surface area, these particles will be easy to extract lithium ions and electrons efficiently during the cycle.

So in this case, it looks like the ionic liquids play key role of both solvent and surface growth directing template agent, and effectively hinder the further growth of precursors and Li_2MnSiO_4/C powders [24]. These two ionic liquids have the same anion [BF_4] but alkyl chains with different lengths on the imidazole ring, which mainly contribute to their diverse properties, such as viscosity, interface tension as listed in Table 1. The viscosity of [EMIM][BF_4] is less than that of [BMIM][BF_4], resulting in the decreased sizes of precursors and final products in [BMIM][BF_4]. It seems that the ionic liquid [BMIM][BF_4] possessing longer alkyl chain of the cation is in favor of smaller nanocrystals. The dissolution and diffusion rate of the ions in the ionic liquid could be slowed down with the increase of the viscosity which increases with alkyl chains lengthening. In addition, the longer the alkyl chains are, the smaller the interfacial tension will be, and consequently the nucleation process will become faster. Owing to the slow dissolution and diffusion, and fast nucleation process, precursor nanocrystals with small size can be easily obtained [25]. However, the size distribution is quite wide, so much larger or smaller individual particles can also be found after calcination process. It indicates that these ionic liquids have different effects on the crystallinity of Li_2MnSiO_4 particle, which result in further differentiation of morphology and particle size followed by calcination.

TEM images in Fig. 5 illustrate that both Li_2MnSiO_4/C-1(a) and Li_2MnSiO_4/C-2(b) are uniformly surrounded by a carbon layer. However, in the same original magnification 200,000×, the crystal lattice stripes of Li_2MnSiO_4/C-2 are observed more clearly. Accompanying with the smaller surface tension of ionic liquid, the surface of the sample becomes smoother, which leads to easier carbon-coating. Furthermore, the profile of the sample does not change obviously, and maintains the irregularly-shaped after carbon-coating. In this article, sucrose as the carbon precursor is employed to improve the electrochemical performance of samples by increasing the electronic conductivity and reducing particle

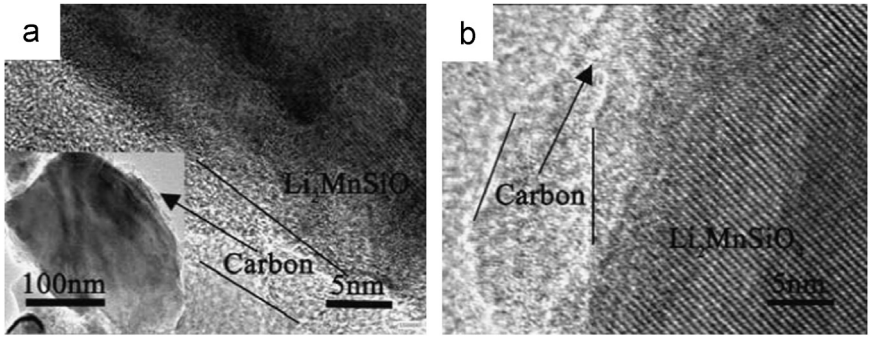

Fig. 5. TEM images of Li_2MnSiO_4/C-1 (a) and Li_2MnSiO_4/C-2 (b) prepared at 750 °C.

agglomeration [17,23]. This technology has been used for improving the electrochemical performance of electrode materials and the feasibility has been verified by the experimental results.

3.3. Electrochemical properties

The electrochemical characteristics of prepared Li_2MnSiO_4/C-1 and Li_2MnSiO_4/C-2 are shown in Fig. 6. Fig. 6(a) and (c) shows the galvanostatic charge–discharge curves of Li_2MnSiO_4/C-1 and Li_2MnSiO_4/C-2 cathode in the potential range of 2.5–4.5 V (vs. Li/Li^+) [10]. In order to prevent the extraction of excessive lithium-ion and protect the structure of solid electrolyte interface (SEI) film, the discharge cut-off voltage was selected at 2.5 V. In Fig. 6(a), Li_2MnSiO_4/C-1 cathode shows the initial discharge capacities of 204, 140, and 79.6 mAh g^{-1} at different current densities of 0.1, 1, and 5 C, respectively. In Fig. 6(c) the Li_2MnSiO_4/C-2 cathode shows larger discharge capacity and lower electrochemical polarization during cycling, and presents the initial charge and discharge capacities at a current density of 0.1 C are determined as 245.1 and 218.2 mAh g^{-1}. The results suggest that the sample prepared in $[BMIM]BF_4$ presents higher crystallinity than that in $[EMIM]BF_4$. This phenomenon can be attributed to the improved structure and the improvement of electrical conductivity [24].

Fig. 6(b) and (d) shows the discharge curves of the Li_2MnSiO_4/C-1 and Li_2MnSiO_4/C-2 samples for 50 cycles at various current densities, i.e., 0.1, 1, and 5 C. It can be seen clearly that the sample with additives exhibits high discharge capacity and low capacity loss ratio. Fig. 5(b) and Table 2 show the cycling performance of the Li_2MnSiO_4/C-1 sample. The capacity faded during cycling with increasing cycle number and stabilized at about 159 mAh g^{-1} after 50 cycles at 0.1 C corresponding to 77.9% of the initial discharge capacity. In Fig. 6(d) and Table 3, the discharge capacity remained about 175.7 mAh g^{-1} after 50 cycles at 0.1 C. This may be attributed to the destruction of the crystal structure during the cycling process which leads to the amorphous state and poor electrical conductivity. Moreover, when the current density is as high as 5 C, Li_2MnSiO_4/C-2 sample presents good electrochemical performance with a reversible capacity of 62.6 mAh g^{-1} after 50 cycles and Li_2MnSiO_4/C-1 sample could only deliver 54.0 mAh g^{-1} in the same conditions. Fig. 6 also reveals that the voltage hysteresis [29] of Li_2MnSiO_4/C-1 electrode is larger than that of Li_2MnSiO_4/C-2 electrode during the discharge and charge process. The reason for this could be explained as follows, the SEI film on Li_2MnSiO_4/C-1 surface becomes thicker and the surface resistance gets higher than those of Li_2MnSiO_4/C-2 electrode, which results in the greater hindrance and higher overvoltage during lithium extraction from electrode. All of the above could be verified by the test of electrochemical impedance spectroscopy (EIS) [29].

The results of first charge–discharge test and discharge curves indicated that the improved electrochemical performance of Li_2MnSiO_4/C mainly resulted from uniform carbon coating, and well-crystallized structure. By analogy with the findings for materials with the orthorhombic $Pmn2_1$ structure, it is possible to speculate on the cause of the capacity fade and the low first discharge capacities. $Pmn2_1$ materials have been found to rapidly lose crystallinity during cycling, resulting in a collapse of the crystal structure and an amorphization of the cathode after several charge–discharge cycles, which have been studied by other investigators [23,30]. Most likely, our better electrochemical performance illustrate that well-selected ionic liquids could be used as structure-directing agents to prepare tailor-made powders, and stabilize polymorphs. It is likely that in this case we found a new way to solve the challenge for the rapid loss in capacity to a certain degree.

3.4. Electrochemical impedance spectroscopy (EIS)

EIS measurements of the prepared Li_2MnSiO_4/C-1 and Li_2MnSiO_4/C-2 nanoparticles were carried out to measure the lithium-ion diffusion coefficient. Fig. 7(a) shows the Nyquist plots of both electrodes. The Nyquist plots can be divided into three regions: an arc is related to the SEI layer and electronic resistance at high frequency, a semicircle is applied to the charge transfer at middle frequency and the straight line is attributed to the diffusion of the lithium ions into the bulk of the electrode material or so-called Warburg diffusion [13] at low frequency. Relevant equivalent circuit is also shown in Fig. 7(a). The resistance contribution from the electrolyte and electrode is represented by R_e. R_f and CPE_1 relate to surface film, CPE_2 represents double layer capacitance, R_{ct} represents the charge transfer resistance of electrochemical reaction and W represents Warburg impedance [31]. The lithium-ion

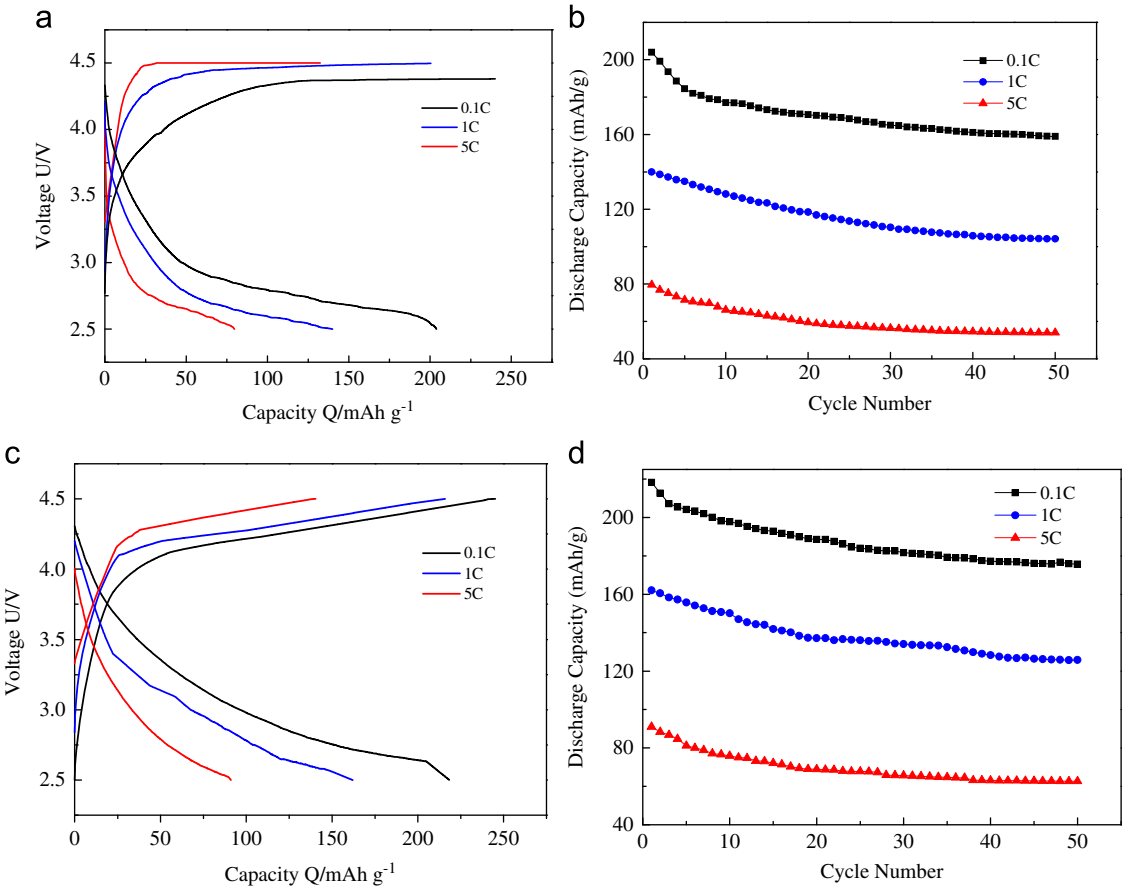

Fig. 6. Charge–discharge curves and cycling performance of the prepared Li_2MnSiO_4/C-1 and Li_2MnSiO_4/C-2 samples, (a) charge–discharge curves of the Li_2MnSiO_4/C-1, (b) cycling performance of the Li_2MnSiO_4/C-1, (c) charge–discharge curves of the Li_2MnSiO_4/C-2, and (d) cycling performance of the Li_2MnSiO_4/C-2.

Table 2
Charge–discharge cycling capacities of Li_2MnSiO_4/C-1 samples.

Current densities (C)	First charge capacities (mAh g^{-1})	First discharge capacities (mAh g^{-1})	50th discharge capacities (mAh g^{-1})	50th discharge capacities retention (%)
0.1	240.0	204.0	159.0	77.9
1	200.4	140.0	104.2	74.4
5	132.4	79.6	54.0	67.8

Table 3
Charge–discharge cycling capacities of Li_2MnSiO_4/C-2 samples.

Current densities (C)	First charge capacities (mAh g^{-1})	First discharge capacities (mAh g^{-1})	50th discharge capacities (mAh g^{-1})	50th discharge capacities retention (%)
0.1	245.1	218.2	175.7	80.5
1	215.8	162.1	125.8	77.6
5	140.4	91.0	62.6	68.8

diffusion coefficient can be calculated from the low frequency line according to the following equation [13,32]:

$$D = \frac{R^2T^2}{2A^2n^4F^4C^2\sigma^2}$$

where R is the gas constant, T is the absolute temperature, A is the surface area of the electrode, n is the number of electrons per molecule during oxidation, F is the Faraday constant, C is the concentration of lithium ion, and σ is the Warburg factor which is related to Z′ by the following [13,32].

$$Z' = B + \sigma\omega^{-1/2}$$

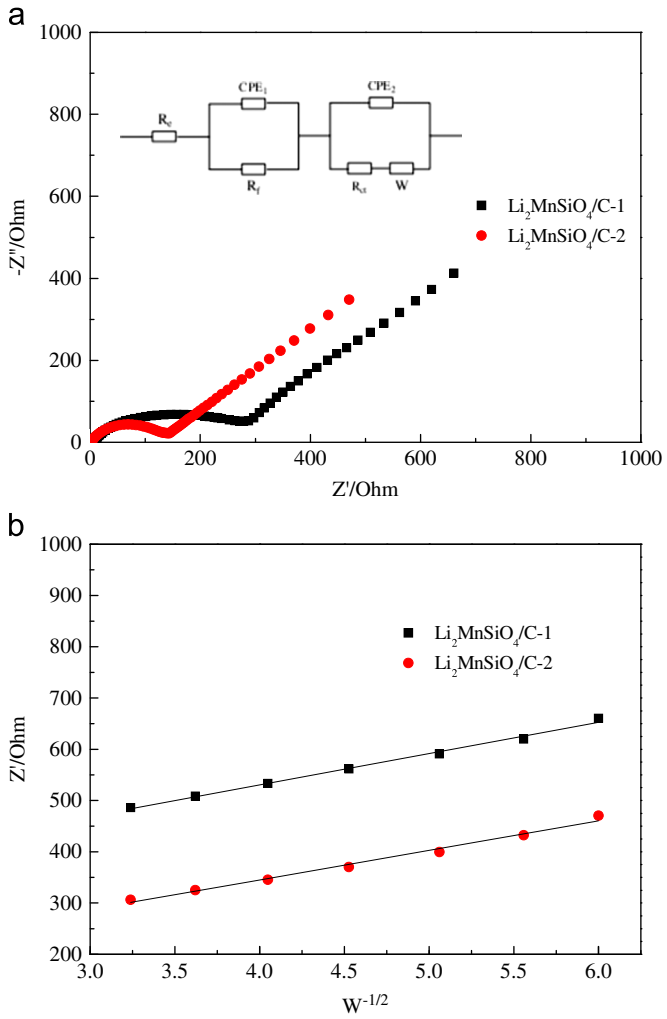

Fig. 7. (a) Nyquist plots of the prepared Li_2MnSiO_4/C-1 and Li_2MnSiO_4/C-2 electrodes and (b) the relationship between Z′ and $\omega^{-1/2}$ in the low-frequency range.

where B is a constant and ω is the frequency. Fig. 7(b) shows the relationships between Z' and the reciprocal square root of frequency in the low-frequency region. The calculated lithium ion diffusion coefficients for both samples are listed in Table 4. Clearly, the high and middle frequency parts of the synthesized Li_2MnSiO_4/C-2 composite materials are smaller than those of the Li_2MnSiO_4/C-1, and the charge transfer resistance of Li_2MnSiO_4/C-2 sample (R_{ct} = 128.3 Ω) is much lower than that of the Li_2MnSiO_4/C-1 sample (R_{ct} = 248.7 Ω). The charge transfer resistance decreases with the increases of electronic conductivity and specific surface area. The sloping line at low frequency is associated with the lithium diffusion in the solid phase, the calculated lithium diffusion coefficients of Li_2MnSiO_4/C-1 and Li_2MnSiO_4/C-2 samples are $5.03(4) \times 10^{-14}$ cm^2 s^{-1} and $7.46(7) \times 10^{-14}$ cm^2 s^{-1}, respectively. It indicates that Li_2MnSiO_4/C-2 particles are more stable and smaller, which can lessen the change of the crystal lattice during the charge–discharge process. This stabilization effect can protect the diffusion path of lithium-ion from being distorted and improve the lithium diffusivity. The lithium

Table 4
Charge transfer resistance and lithium ion diffusion coefficient of Li_2MnSiO_4/C-1 and Li_2MnSiO_4/C-2.

Sample	Charge transfer resistance (R_{ct} Ω)	Lithium ion diffusion coefficient(cm^2 s^{-1})
Li_2MnSiO_4/C-1	248.7	$5.03(4) \times 10^{-14}$
Li_2MnSiO_4/C-2	128.3	$7.46(7) \times 10^{-14}$

diffusion coefficient of Li_2MnSiO_4/C-2 composites exhibits a larger value, which indicates the electrons and Li^+ ions can transfer more quickly on the interface of electrode/electrolyte. As is well known, it is important for a cathode material to achieve good electrochemical performance.

4. Conclusions

Uniformly dispersed Li_2MnSiO_4 precursors are prepared by recyclable ionothermal synthesis under the mild conditions of low-temperature and ambient pressure by using imidazolium-based [EMIM]BF_4 and [BMIM]BF_4 ionic liquids as the reaction mediums. The effect of the properties of [BMIM]BF_4 such as higher viscosity, smaller interfacial tension on the morphologies and size of the product are studied. Compared with Li_2MnSiO_4/C-1 sample, the Li_2MnSiO_4/C-2 exhibits smaller size and favorable electrochemical properties such as high-rate ability and cycling stability with a maximum discharge capacity of 218.2 mAh g^{-1} and a reversible capacity of 175.7 mAh g^{-1} in the 50th cycle. The excellent performance of materials are mainly ascribed to the special role of ionic liquid owing to its ability of improving dispersion and decreasing size, and good electronic conductivity of carbon coating. Results demonstrate that ionothermal synthesis can provide effective strategy for synthesizing cathode material such as orthosilicate with uniform size and excellent electrochemical performance.

Acknowledgments

This work was financially supported by the 2010 Annual Key Project of Anhui Province of China (No. KJ2010A278) and the Science and Technology Project of Land and Resources of Anhui Province (2010-g-19, 2011-k-11).

References

[1] S. Luo, K. Wang, J. Wang, K. Jiang, Q. Li, S. Fan, Binder-free $LiCoO_2$/Carbon nanotube cathodes for high-performance lithium ion batteries, Advanced Materials 24 (17) (2012) 2294–2298.
[2] J. Yao, L. Lv, C. Shen, P. Zhang, K.-F. Aguey-Zinsou, L. Wang, Nano-sized spinel $LiMn_2O_4$ powder fabricated via modified dynamic hydrothermal synthesis, Ceramics International 39 (3) (2013) 3359–3364.
[3] G.B. Cho, H.J. Choe, B.M. Kim, H.J. Mun, J.P. Noh, T.H. Nam, Electrochemical and mechanical properties of superelastic electrode consisting of Ti substitute $LiNiO_2$ film on Ti–50Ni alloy, Journal of Alloys and Compounds 488 (1) (2009) L17–L20.

[4] A.K. Padhi, K.S. Nanivndaswamy, J.B. Goodenough, Phospho-olivines as positive-electrode materials for rechargeable lithium batteries, Journal of the Electrochemical Society 144 (4) (1997) 1188–1194.
[5] C. Deng, S. Zhang, B.L. Fu, S.Y. Yang, L. Ma, Characterization of Li_2MnSiO_4 and Li_2FeSiO_4 cathode materials synthesized via a citric acid assisted sol–gel method, Materials Chemistry and Physics 120 (1) (2010) 14–17.
[6] G. Zhong, Y. Li, P. Yan, Z. Liu, M. Xie, H. Lin, Structural, electronic, and electrochemical properties of cathode materials Li_2MSiO_4 (M=Mn, Fe, and Co): density functional calculations, Journal of Physical Chemistry C 114 (8) (2010) 3693–3700.
[7] D. Santamaria-Perez, U. Amador, J. Tortajada, R. Dominko, M. E. Arroyo-de Dompablo, High-Pressure investigation of Li_2MnSiO_4 and Li_2CoSiO_4 electrode materials for lithium–ion batteries, Inorganic Chemistry 51 (10) (2012) 5779–5786.
[8] S. Luo, M. Wang, W. Sun, Fabricated and improved electrochemical properties of Li_2MnSiO_4 cathodes by hydrothermal reaction for Li-ion batteries, Ceramics International 38 (5) (2012) 4325–4329.
[9] V.V. Politaev, A.A. Petrenko, V.B. Nalbandyan, B.S. Medvedev, E. S. Shvetsova, Crystal structure, phase relations and electrochemical properties of monoclinic Li_2MnSiO_4, Journal of Solid State Chemistry 180 (3) (2007) 1045–1050.
[10] R.J. Gummow, N. Sharma, V.K. Peterson, Y. He, Crystal chemistry of the Pmnb polymorph of Li_2MnSiO_4, Journal of Solid State Chemistry 188 (2012) 32–37.
[11] X.Y. Fan, Y. Li, J.J. Wang, L. Gou, P. Zhao, D.L. Li, L. Huang, S. G. Sun, Synthesis and electrochemical performance of porous Li_2FeSiO_4/C cathode material for long-life lithium-ion batteries, Journal of Alloys and Compounds 493 (1–2) (2010) 77–80.
[12] W. Liu, Y. Xu, R. Yang, Synthesis, characterization and electrochemical performance of Li_2MnSiO_4/C cathode material by solid-state reaction, Journal of Alloys and Compounds 480 (2) (2009) L1–L4.
[13] S. Zhang, C. Deng, B.L. Fu, S.Y. Yang, L. Ma, Effects of Cr doping on the electrochemical properties of Li_2FeSiO_4 cathode material for lithium-ion batteries, Electrochimica Acta 55 (28) (2010) 8482–8489.
[14] M.E. Arroyo-de Dompablo, M. Armand, J.M. Tarascon, U. Amador, On-demand design of polyoxianionic cathode materials based on electronegativity correlations: an exploration of the Li_2MSiO_4 system (M=Fe, Mn, Co, Ni), Electrochemistry Communications 8 (8) (2006) 1292–1298.
[15] R. Dominko, M. Bele, M. Gaberscek, A. Meden, M. Remskar, J. Jamnik, Structure and electrochemical performance of Li_2MnSiO_4 and Li_2FeSiO_4 as potential Li-battery cathode materials, Electrochemistry Communications 8 (2) (2006) 217–222.
[16] K. Karthikeyan, V. Aravindan, S.B. Lee, I.C. Jang, H.H. Lim, G.J. Park, M. Yoshio, Y.S. Lee, Electrochemical performance of carbon-coated lithium manganese silicate for asymmetric hybrid supercapacitors, Journal of Power Sources 195 (11) (2010) 3761–3764.
[17] P. Ghosh, S. Mahanty, R.N. Basu, Improved electrochemical performance of Li_2MnSiO_4/C composite synthesized by combustion technique, Journal of the Electrochemical Society 156 (8) (2009) A677–A681.
[18] V. Aravindan, K. Karthikeyan, K.S. Kang, W.S. Yoon, W.S. Kim, Y. S. Lee, Influence of carbon towards improved lithium storage properties of Li_2MnSiO_4 cathodes, Journal of Materials Chemistry 21 (8) (2011) 2470–2475.
[19] V. Aravindan, S. Ravi, W.S. Kim, S.Y. Lee, Y.S. Lee, Size controlled synthesis of Li_2MnSiO_4 nanoparticles: effect of calcination temperature and carbon content for high performance lithium batteries, Journal of Colloid and Interface Science 355 (2) (2011) 472–477.
[20] S. Zhang, C. Deng, S. Yang, Preparation of nano-Li_2FeSiO_4 as cathode material for lithium-ion batteries, Electrochemical and Solid State Letters 12 (7) (2009) A136–A139.
[21] Z.L. Gong, Y.X. Li, Y. Yang, Synthesis and characterization of $Li_2Mn_xFe_{1-x}SiO_4$ as a cathode material for lithium-ion batteries, Electrochemical and Solid State Letters 9 (12) (2006) A542–A544.
[22] S. Zhang, Z. Lin, L. Ji, Y. Li, G. Xu, L. Xue, S. Li, Y. Lu, O. Toprakci, X. Zhang, Cr-doped Li_2MnSiO_4/carbon composite nanofibers as high-energy cathodes for Li-ion batteries, Journal of Materials Chemistry 22 (29) (2012) 14661–14666.
[23] R. Dominko, Li_2MSiO_4 (M=Fe and/or Mn) cathode materials, Journal of Power Sources 184 (2) (2008) 462–468.
[24] N. Recham, L. Dupont, M. Courty, K. Djellab, D. Larcher, M. Armand, J. M. Tarascon, Ionothermal synthesis of tailor-made $LiFePO_4$ powders for Li-ion battery applications, Chemistry of Materials 21 (6) (2009) 1096–1107.
[25] J. Liu, X. Liu, X. Kong, H. Zhang, Controlled synthesis, formation mechanism and upconversion luminescence of $NaYF_4$: Yb, Er nano-/submicrocrystals via ionothermal approach, Journal of Solid State Chemistry 190 (2012) 98–103.
[26] X.L. Li, J.J. Chen, M. Luo, X.Y. Chen, P.P. Li, Quantum chemical calculation of hydroxyalkyl ammonium functionalized ionic liquids for absorbing SO_2, Acta Physico-Chimica Sinica 26 (5) (2010) 1364–1372.
[27] M.E.Arroyo y de Dompablo, U. Amador, J.M. Gallardo-Amores, E. Moran, H. Ehrenberg, L. Dupont, R. Dominko, Polymorphs of Li_3PO_4 and Li2MSiO4 (M=Mn, Co) the role of pressure, Journal of Power Sources 189 (1) (2009) 638–642.
[28] J.C. Groen, L.A.A. Peffer, J. Perez-Ramirez, Pore size determination in modified micro- and mesoporous materials, pitfalls and limitations in gas adsorption data analysis, Microporous and Mesoporous Materials 60 (1–3) (2003) 1–17.
[29] S. Yang, J. Huo, H. Song, X. Chen, A comparative study of electrochemical properties of two kinds of carbon nanotubes as anode materials for lithium ion batteries, Electrochimica Acta 53 (5) (2008) 2238–2244.
[30] A. Kokalj, R. Dominko, G. Mali, A. Meden, M. Gaberscek, J. Jamnik, Beyond one-electron reaction in Li cathode materials: designing $Li_2Mn_xFe_{1-x}SiO_4$, Chemistry of Materials 19 (15) (2007) 3633–3640.
[31] Z. Feng, J. Yang, Y. NuLi, J. Wang, Sol–gel synthesis of $Mg_{1.03}Mn_{0.97}SiO_4$ and its electrochemical intercalation behavior, Journal of Power Sources 184 (2) (2008) 604–609.
[32] C. Deng, S. Zhang, S.Y. Yang, B.L. Fu, L. Ma, Synthesis and characterization of $Li_2Fe_{0.97}M_{0.03}SiO_4$ (M=Zn^{2+}, Cu^{2+}, Ni^{2+}) cathode materials for lithium ion batteries, Journal of Power Sources 196 (1) (2011) 386–392.